Nat. Hazards Earth Syst. Sci. Discuss., 3, 6651–6688, 2015
www.nat-hazards-earth-syst-sci-discuss.net/3/6651/2015/
doi:10.5194/nhessd-3-6651-2015

Natural Hazards and Earth System Sciences
Discussions

GPS derived ground motions (2005–2014) within the Gulf of Mexico region referred to a stable Gulf of Mexico reference frame

J. Yu and G. Wang

Department of Earth and Atmospheric Sciences, National Center for Airborne LiDAR Mapping, University of Houston, Houston, Texas, USA

Received: 27 August 2015 – Accepted: 4 October 2015 – Published: 3 November 2015

Correspondence to: J. Yu (jyu7@uh.edu)

Published by Copernicus Publications on behalf of the European Geosciences Union.

Abstract

This study investigates current ground motions derived from the GPS geodesy infrastructure in the Gulf of Mexico region. The positions and velocity vectors of 161 continuous GPS (CGPS) stations are presented with respect to a newly established local reference frame, the Stable Gulf of Mexico Reference Frame (SGOMRF). Thirteen long-term (> 5 years) CGPS are used to realize the local reference frame. The root-mean-square (RMS) of the velocities of the 13 SGOMRF reference stations achieves 0.2 mm yr^{-1} in the horizontal and 0.3 mm yr^{-1} in the vertical directions. GPS observations presented in this study indicate significant land subsidence in the coastal area of southeastern Louisiana, the greater Houston metropolitan area, and two cities in Mexico (Aguascalientes and Mexico City). The most rapid subsidence is recorded at the Mexico City International airport, which is up to 26.6 cm yr^{-1} (2008–2014). Significant spatial variation of subsidence rates is observed in both Mexico City and the Houston area. The overall subsidence rate in the Houston area is decreasing. GPS observations in southeastern Louisiana indicate minor (4.0–6.0 mm yr^{-1}) but consistent subsidence over time and space. This poses a potential threat to the safety of costal infrastructure in the long-term.

1 Introduction

The Gulf of Mexico (GOM) region consists of the Mexico Gulf Coast and the US Gulf States. The US Gulf States include Texas, Louisiana, Mississippi, Alabama, and Florida. This region has been the heart of the US energy industry because of substantial oil and gas deposits along the coast and offshore of the GOM. It is heavily populated and vulnerable to local ground deformation (faulting, subsidence, uplift) and relative sea-level rise (e.g., Day et al., 1995; Kolker et al., 2011; Thatcher et al., 2013). Land subsidence and faulting problems in the GOM region have been frequently investigated by different research groups using GPS observations (e.g., Dokka, 2011;

NHESSD
3, 6651–6688, 2015

Engelkemeir et al., 2010; Kearns et al., 2015; Khan et al., 2014; Osmanoglu et al., 2011; Wang and Soler, 2013). However, it is difficult to align the results from these research groups because they used different data sets collected by different organizations during different time periods. Furthermore, they focused on localized ground deformation and applied different reference points or frames. This study aims to establish a unified local geodetic reference frame, the Stable Gulf of Mexico Reference Frame (SGOMRF), to investigate the current ground motion within the whole GOM region during the past decade (2005–2014). Long-term observations from about 450 continuous GPS (CGPS) stations are investigated (Fig. 1). Land subsidence, faulting, and salt dome activities in the Houston region, Mexico City, and the southeastern Louisiana region are discussed and compared.

2 GPS data processing

This study applies the Precise Point Positioning (PPP) method, for solving the 24 h average position of a GPS antenna. PPP is based on the processing of the following ionosphere-free combinations of the undifferenced code and phase observations (Zumberge et al., 1997):

$$P_{\mathrm{IF}} = \frac{f_1^2 \cdot P(\mathrm{L1}) - f_2^2 \cdot P(\mathrm{L2})}{f_1^2 - f_2^2} = \rho - c \cdot \mathrm{d}T + d_{\mathrm{trop}} \quad (1)$$

$$\Phi_{\mathrm{IF}} = \frac{f_1^2 \cdot \Phi(\mathrm{L1}) - f_2^2 \cdot \Phi(\mathrm{L2})}{f_1^2 - f_2^2} = \rho - c \cdot \mathrm{d}T + d_{\mathrm{trop}} + \frac{cf_1 N_1' - cf_2 N_2'}{f_1^2 - f_2^2} \quad (2)$$

where f_1 and f_2 are the GPS L1 and L2 frequencies; $P(\mathrm{L}i)$ and $\Phi(\mathrm{L}i)$ are the code and phase observations at the corresponding frequency; ρ is the true range; c is the speed of light; $\mathrm{d}T$ is the receiver clock offset; d_{trop} is the tropospheric delays; N_i' is

NHESSD
3, 6651–6688, 2015

the phase ambiguity term in $\Phi(L_i)$. Therefore, the unknown parameters estimated in PPP include position coordinates, phase ambiguity, receiver clock offset and the tropospheric delays. GNSS-Inferred Positioning System and Orbit Analysis Simulation Software (GIPSY-OASIS) package (V6.3) developed at the Jet Propulsion Laboratory (JPL) is applied for calculating daily positions. The GIPSY-OASIS package provides single receiver phase ambiguity fixed PPP solutions. The single receiver phase ambiguity method uses the wide lane and phase bias estimates obtained from a global network of ground GPS stations to perform ambiguity-resolved PPP resolution (Bertiger et al., 2010). The major parameters estimated and key models applied in the PPP processing include: the VMF1 troposphere mapping model (Boehm et al., 2006), second order ionospheric delay (Kedar, 2003), the ocean tidal loading model FES2004 (Lyard et al., 2006) calculated through the free online service operated by Onsala Space Observatory, Sweden (The free ocean tide loading provider, 2015), tropospheric gradient (Bar-Sever et al., 1998), zenith troposphere delay as a random walk with variance of $5 \times 10^{-8}\,\mathrm{km\,s^{-2}}$, gradient troposphere wet delay as a random walk with variance of $5 \times 10^{-9}\,\mathrm{km\,s^{-2}}$, and receiver clock as white noise with updates every measurement epoch. Station coordinates are initially provided in the loose frame of the JPL's fiducial-free GPS orbits. The coordinates are then transformed into the International GNSS Service Reference Frame of 2008 (IGS08) using the daily seven transformation parameters that are delivered with the JPL's orbit products.

The PPP processing conducts all calculations within an Earth-Centered-Earth-Fixed (ECEF) geocentric coordinate system (x, y, and z). In order to track land surface deformation, the ECEF geocentric coordinates are converted to cartographic (northing, easting, and ellipsoidal height) coordinates, which are referred to the GRS-80 ellipsoid. The three-component daily positional time series indicates the change of ground surface over time at different directions. The three components represent: north to south (NS), east to west (EW), and up to down (UD). The UD component (subsidence/uplift) measurements used in this study are obtained by differencing GPS measured ellipsoidal heights referred to the local reference frame. Detection of regional-scale land

NHESSD
3, 6651–6688, 2015

subsidence has historically depended on surveying benchmarks periodically. This has traditionally been accomplished by differencing orthometric heights obtained from spirit leveling. A recent investigation conducted by Wang and Soler (2014) has indicated that using ellipsoid and orthometric heights would result in the same practical subsidence measurements. Accordingly, the subsidence values used in this study can be regarded as having the same "physical meaning" as the conventional subsidence measurements obtained from leveling surveys. An outlier identifying and removing approach developed by Firuzabadì and King (2011) and Wang (2011) was implemented to identify and remove outliers. On average, five percent of the total samples are removed as outliers. The daily positional time series applied in this article are the "cleaned" time series.

3 Stable Gulf of Mexico Reference Frame (SGMRF)

In general, a global or a continental-scale reference frame is realized with an approach of minimizing the least square residual velocities of a large number of selected reference stations (Altamimi et al., 2007; DeMets et al., 1990). In the case of IGS08, 232 globally-distributed, and well-performing GPS stations are used (Rebischung et al., 2012). The velocities at GPS sites referred to IGS08 are dominated by tectonic drift. For a regional study, a stable local reference frame is often established through Helmert transformation to exclude tectonic drift (Wang et al., 2013, 2014, 2015). It facilitates the precise physical interpretation of local ground deformation over time and space. The transformation involves 7 parameters including rotation vector, translation vector and differential scale factor. The transformation parameters can be estimated by comparing the positions of a group of selected reference stations referred to the new reference frame with those referred to a well-established reference frame.

In practice, at least three reference stations are needed to obtain the transformation parameters. More reference stations often result in higher accuracy. However, a reference station that is not locally stable will degrade the overall accuracy of the reference frame. A stable site is defined as retaining zero velocities (three components) with re-

NHESSD
3, 6651–6688, 2015

spect to a specified reference frame. The stability (precision) of a local reference frame is therefore affected by the velocities of stable sites with respect to the reference frame. Thus, the selection of reference stations is critical for establishing a stable local reference frame. In general, there is not a fixed criterion for selecting reference stations. The selection mostly is based on the availability of long-term CGPS stations in the study area. There are over 780 CGPS stations in the GOM region (Fig. 1). As this study uses a secular frame, the linearity of daily positional time series is a critical criteria for selecting reference stations (Blewitt and Lavallée, 2002). Additionally, the geographic distribution of reference stations as a group is also considered. The following specific criteria are initially applied for selecting reference stations:

1. having segments of data spanning at least 5 years (installed in 2009 or earlier) with no steps (a sharp change of the mean in positional time series caused by an earthquake, equipment change, or other unknown reasons);

2. no considerable subsidence or uplifting (the linear velocity rate of vertical positional time series referred to IGS08 is less than 0.5 mm yr^{-1});

3. having less than 0.1 mm yr^{-1} "standard error" (σ) of the linear regression in calculating the slope (V_{cal}) of the geocentric coordinate time series (x, y, and z) referred to IGS08. σ represents the average difference between the observed values and the regression line. Approximately 95 % of the time, the true velocity will be contained in the interval between $V_{cal} - 1.96 \times \sigma$ and $V_{cal} + 1.96 \times \sigma$.

The near-coast areas could be affected by subsidence and coastal erosion problems (Simms et al., 2013; Williams et al., 1997; Yu et al., 2014). Accordingly, it is preferred that reference stations be located inland rather than within near-coast areas. However, in order to balance the overall coverage and geometrical distribution of reference stations, one near-coast station in Florida (RMND) and one near-coast station in Mexico (TAM1) were selected as reference stations (Fig. 2). Uneven distribution of reference sites could lead to biases in frame transformation (Collilieux et al., 2010; Wang et al.,

NHESSD
3, 6651–6688, 2015

2014). Positional time series affected by steps are identified by an automated edge detection program based on the derivative of Gaussian kernel (Canny, 1986). Initially, 30 CGPS stations were selected then a try-out procedure was employed to refine the selection. Any reference station with a horizontal velocity greater than 1 mm yr^{-1} referred to the local reference frame was removed from the group of reference stations. The reference frame transformation parameters were then recalculated. Finally, 13 CGPS stations are selected as reference stations for realizing the SGOMRF (Fig. 2).

Two different approaches are often used in geodesy to transform positional time series from one reference frame to another: the daily 7-parameter Helmert transformation and the 14-parameter similarity transformation. This study applies a 14-parameter transformation approach that is widely used in the geodesy surveying community (e.g., Pearson and Snay, 2012; Wang et al., 2014). The geocentric coordinates of a station with respect to SGOMRF are calculated by the following formulas:

$$
\begin{aligned}
X(t)_{\mathrm{SGOMRF}} &= T_X(t) + [1 + s(t)] \cdot X(t)_{\mathrm{IGS08}} + R_Z(t) \cdot Y(t)_{\mathrm{IGS08}} - R_Y(t) \cdot Z(t)_{\mathrm{IGS08}} \\
Y(t)_{\mathrm{SGOMRF}} &= T_Y(t) - R_Z(t) \cdot X(t)_{\mathrm{IGS08}} + [1 + s(t)] \cdot Y(t)_{\mathrm{IGS08}} + R_X(t) \cdot Z(t)_{\mathrm{IGS08}} \\
Z(t)_{\mathrm{SGOMRF}} &= T_Z(t) + R_Y(t) \cdot X(t)_{\mathrm{IGS08}} - R_X(t) \cdot Y(t)_{\mathrm{IGS08}} + [1 + s(t)] \cdot Z(t)_{\mathrm{IGS08}}. \qquad (3)
\end{aligned}
$$

Here, $T_x(t)$, $T_Y(t)$ and $T_Z(t)$ are translations along X, Y and Z axis; $R_X(t) R_Y(t)$ and $R_Z(t)$ are counterclockwise rotations about three axes; $s(t)$is a differential scale factor between IGS08 and SGOMRF. These seven parameters at a specific epoch can be calculated by the following formulas:

NHESSD
3, 6651–6688, 2015

$$
\begin{aligned}
T_X(t) &= T_X(t_0) + \mathrm{d}T_X \cdot (t - t_0) \\
T_Y(t) &= T_Y(t_0) + \mathrm{d}T_Y \cdot (t - t_0) \\
T_Z(t) &= T_Z(t_0) + \mathrm{d}T_Z \cdot (t - t_0) \\
R_X(t) &= R_X(t_0) + \mathrm{d}R_X \cdot (t - t_0) \\
R_Y(t) &= R_Y(t_0) + \mathrm{d}R_Y \cdot (t - t_0) \\
R_Z(t) &= R_Z(t_0) + \mathrm{d}R_Z \cdot (t - t_0) \\
s(t) &= s(t_0) + \mathrm{d}s \cdot (t - t_0) .
\end{aligned} \tag{4}
$$

Here, t_0 denotes a specific epoch (e.g., 2013.0). $T_X(t_0)$, $T_Y(t_0)$, $T_Z(t_0)$, $R_X(t_0)$, $R_Y(t_0)$, $R_Z(t_0)$ and $s(t_0)$ are the seven transformation parameters at epoch t_0. The two reference frames are aligned at epoch 2013.0. That means the positional coordinates of a site with respect to both reference frames are identical at this epoch. Thus, the seven transformation parameters at epoch t_0 are all zeros. $\mathrm{d}T_X$, $\mathrm{d}T_Y$, $\mathrm{d}T_Z$, $\mathrm{d}R_X$, $\mathrm{d}R_Y$, $\mathrm{d}R_Z$ and $\mathrm{d}s$ are the first-time derivatives of corresponding parameters, which are constant over time. The units of these parameters are meters for translational components, radians for rotational components, $\mathrm{m\,yr^{-1}}$ for the rate of translational movement, and $\mathrm{radian\,yr^{-1}}$ for the rate of rotational components. $s(t)$ is a unitless scale factor. The unit of $\mathrm{d}s$ is $\mathrm{yr^{-1}}$. The 14 parameters for coordinate transformation from the IGS08 to the SGOMRF are listed in Table 1. The detailed method of obtaining these 14 parameters was explained in Wang et al. (2014), which established a stable local reference frame in the Puerto Rico and Virgin Islands region for local faulting and landslide studies.

Figure 3 depicts the three-component positional time series of two stations (OKAN and SG05) referred to SGOMRF, North American Datum of 1983 (NAD 83) (2011) and IGS08. The NAD 83 is the horizontal control datum for the US, Canada, Mexico, and Central America (Schwarz, 1989; Snay and Soler, 2000). It is widely used as a North American plate-fixed reference frame in the practice of surveying. The continental-scale reference frame has been updated for several times. The most recent realization is referred as NAD83(2011) at epoch 2010.0. The positional coordi-

NHESSD
3, 6651–6688, 2015

nates referred to NAD83(2011) are transformed from IGS08 with Eqs. (3) and (4) and 14 parameters provided by Pearson and Snay (2012) (Table 1). Both sites retain near-zero velocities ($< 0.5\,\mathrm{mm\,yr^{-1}}$) with respect to the local reference frame SGOMRF. The three-component velocities derived from the 10 year (2004–2014) continuous observations at OKAN are $-2.3\,\mathrm{mm\,yr^{-1}}$ (NS), $-13.4\,\mathrm{mm\,yr^{-1}}$ (EW), and $0.2\,\mathrm{mm\,yr^{-1}}$ (UD) with respect to IGS08 and $0.6\,\mathrm{mm\,yr^{-1}}$ (NS), $1.6\,\mathrm{mm\,yr^{-1}}$ (EW), and $-0.2\,\mathrm{mm\,yr^{-1}}$ (UD) with respect to NAD83. The velocities at SG05 are generally the same (Fig. 3). Thus both sites are not "stable" with regard to IGS08 and NAD83. The horizontal velocity ($1.5\,\mathrm{cm\,yr^{-1}}$) referred to IGS08 can be explained by the tectonic movement of the GOM region with respect to the global reference frame. However the minor horizontal movements ($\sim 2\,\mathrm{mm\,yr^{-1}}$) with respect to the supposedly continent-fixed reference frame (NAD83) can be misleading. The same minor horizontal movements with respect to NAD83(2011) can also be observed at the 13 reference stations, even though the near-zero velocities with respect to SGOMRF indicate they are stable (Fig. 2). The coherent horizontal movement referred to the NAD83(2011) could be easily and incorrectly interpreted as the result of local faulting activities. In fact, the $2\,\mathrm{mm\,yr^{-1}}$ horizontal velocity does not represent any local ground movement. It indicates the instability of the NAD83 reference frame within the GOM region. The instability of the continental-scale reference frame will overlook or bias minor local horizontal ground deformation signals.

The root-mean-square (RMS) value of the 13 reference stations' velocities are $0.15\,\mathrm{mm\,yr^{-1}}$ for the EW component, $0.19\,\mathrm{mm\,yr^{-1}}$ for the NS component, and $0.25\,\mathrm{mm\,yr^{-1}}$ for vertical component with respect to the local reference frame (SGOMRF). This suggests that the stability of SGOMRF is at the level of $0.2\,\mathrm{mm\,yr^{-1}}$ in the horizontal and $0.3\,\mathrm{mm\,yr^{-1}}$ in the vertical directions. Table 2 lists the average coordinates of these 13 reference stations referred to SGOMRF at epoch 2013.0 and the RMS values of corresponding residual time series. These RMS values are often regarded as the precision (repeatability) of the daily positions. The results illustrated in Table 2 suggest that the PPP solutions obtained in this study achieve 2 mm horizontal precision and 7 mm vertical precision, which is comparable with the overall precision

NHESSD
3, 6651–6688, 2015

of GIPSY-OASIS PPP solutions. Bertiger et al. (2010) reported that the single receiver ambiguity fixed PPP solutions achieved overall 2 mm horizontal precision and 6 mm vertical precision for the 106 worldwide IGS reference stations.

4 Horizontal ground deformation

We selected 148 stations that have step-free time spans of longer than four years, and transform the daily positional time series to the local reference frame (Fig. 4). The average horizontal velocity of these 148 stations is below 1 mm yr^{-1}, which implies that the rigidity of the GOM region is at the level of sub-millimeter per year. Five long-term GPS stations have been moving horizontally with relatively larger velocities (> 2 mm yr^{-1}). These stations are MMX1 (9.7 mm yr^{-1}), FSHS (3.4 mm yr^{-1}), UNIP (2.9 mm yr^{-1}), TXPR (2.4 mm yr^{-1}) and ROD1 (2.4 mm yr^{-1}). Four of these stations are located in well-known subsidence areas. MMX1 is located in Mexico City, Mexico. FSHS is located in Franklin, Louisiana. UNIP is located in Aguascalientes, Mexico. ROD1 is located in Houston, Texas.

In the case of groundwater withdrawal induced subsidence, a subsidence bowl can be formed by localized aquifer compaction. In such an event, it is possible that GPS stations are pulled slightly towards the center of the subsidence bowl. Depending on the position of a station relative to the subsidence center, the ratio of horizontal to vertical velocities varies. A station at the edge of the subsidence center will show a relatively large horizontal velocity. A station located closer to the center of subsidence could display large velocities in both the horizontal and vertical components. Around the center of the subsidence feature, the stations will mostly exhibit vertical movement. Figure 5 depicts the three-component positional time series at ROD1, TXCN, and TXLI referred to the local reference frame. TXLI is a stable station located in Liberty County, TX. ROD1 shows a 2.3 mm yr^{-1} horizontal movement towards the northeast. TXCN shows no movement in the horizontal direction. Both ROD1 and TXCN indicate long-term subsidence. According to our previous studies on the current subsi-

NHESSD
3, 6651–6688, 2015

dence in the greater Houston metropolitan area (Kearns et al., 2015; Yu et al., 2014), a rapid-subsidence bowl is forming around The Woodlands area. The Woodlands is a vibrant and fast-growing business and entertainment suburban located 43 km north of downtown Houston (Fig. 6). Groundwater is the sole water source for residential and business use in this area as of 2014. The subsidence rate in the center of the subsidence bowl is about 25 mm yr^{-1} (Kearns et al., 2015). ROD1 is located in the city of Spring, TX, northern Harris County. The station is 12 km southwest to The Woodlands area (Fig. 6). The subsidence rate at ROD1 is 17 mm yr^{-1} derived from the whole time series from 2007 to 2014. The horizontal velocity vector indicates that ROD1 is moving towards the center of the subsidence bowl, The Woodlands area. TXCN is located in the city of Conroe, TX, which is 21 km north of The Woodlands. The positional time series (2008–2014) of TXCN does not indicate any considerable horizontal movement (< 1 mm yr^{-1}). However, steady land subsidence with a rate of 16 mm yr^{-1} has been recorded at this site. The different vertical-to-horizontal velocity ratio suggests that TXCN is close to the bottom part of the subsidence bowl whereas ROD1 is more likely located along the steep sidewall of the subsidence bowl. The comparison of the three-component positional time series of ROD1 with those of TXCN illustrates a good example of horizontal velocity variations around a subsidence bowl.

A similar movement pattern at two CGPS sites around a subsidence bowl is also observed in Mexico City (Fig. 7). MMX1 is located in the Mexico International Airport, which is located within the eastern portion of Mexico City. UNIP is located at the Universidad Nacional Autónoma de México, which is located within the southwestern portion of Mexico City. The steady 9.7 mm yr^{-1} horizontal movement towards the northeast implies that MMX1 is not at the center of the subsidence bowl. UNIP records a smaller rate of 2.9 mm yr^{-1} towards the northeast. Observations from InSAR indicated that subsidence rates in Mexico City increased eastwards towards the center of the Basin of Mexico (Chaussard et al., 2014). The horizontal movements of MMX1 and UNIP agree well with the subsidence bowl illustrated by the InSAR data: both UNIP and MMX1 are

NHESSD
3, 6651–6688, 2015

moving toward the center of the subsidence bowl; MMX1 is located much closer to the center and therefore has demonstrated higher rates of horizontal motion (Fig. 7).

Figure 8 depicts that FSHS, a permanent GPS station (2010–2014) located at Franklin, Louisiana, has been moving toward the southeast at a rate of 3.4 mm yr^{-1}. The antenna of FSHS is mounted to a reinforced concrete building located at Franklin High School. Subsidence at this site is minor (3.4 mm yr^{-1}). There is no known excessive groundwater withdrawal issue in this area. It is not likely that the horizontal movement is associated with an on-going subsidence bowl. One possible explanation for the horizontal movement at this site is the existence of the South Louisiana Allochthon (SLA) proposed by Dokka et al. (2006). Massive sediment deposition and loading have caused the edge of the continent to become gravitationally instable. The tectonic model indicates that the gravitational instability and sea level rise is causing the SLA to be detached from the stable North American plate and move to south-southeast. FSHS is located at the breakaway zone described in Dokka et al. (2006). It consists of a zone of high-angle, down-to-the-south, listric normal faults. Both the horizontal and vertical movements recorded by FSHS could be caused by faulting at the breakaway zone. Though the data from FSHS (coordinates: 29.81°, −91.50°) started at 2010 and therefore was not used in Dokka et al. (2006), a nearby campaign GPS station FRAN (coordinates: 29.80°, −91.53°), was reported to be moving southward at a rate of 5 mm yr^{-1}. This rate is comparable to the site velocity at FSHS obtained from this study (3.4 mm yr^{-1}). Dokka et al. (2006) used a stable North American reference frame defined by a least squares inversion of the IGb00 velocities for 124 stable CGPS sites. The difference in velocity is more likely caused by the use of different reference frames. Our other GPS sites (AWES, DSTR, HOUM, GRIS, BVHS, LMCN) in southeastern Louisiana also demonstrate movements southward with rates smaller than FSHS. TXPR, a permanent GPS site (2005–2014) located at Pharr, TX, has a horizontal southwest movement of 2.4 mm yr^{-1} (Fig. 8). The antenna pole is anchored on a wall of an office building owned by the Texas Department of Transportation. GPS observations also show steady subsidence (5.8 mm yr^{-1}) at this site. The horizontal

NHESSD
3, 6651–6688, 2015

movement could be associated with local subsidence. Further study is needed to verify the cause of the horizontal motion.

Growth faults are common in the GOM region. The majority of the coastal growth fault systems are located onshore (Fig. 9). The faults dip steeply at 50 to 60° in the upper near-surface, but flatten out with increasing depth. These fault systems break the region into giant polygonal blocks (Worral and Sigmund, 1989). Each polygon may move independently of its neighbors. In southern Texas, numerous growth faults have been documented at depths over 1000 m (Verbeek et al., 1979). Also, there are numerous reports of infrastructure (highways, pipelines, and bridges) and building damage associated with shallow fault creep in the Houston metropolitan area, as well as in New Orleans area. Previous explanations for the cause of the shallow faulting have emphasized groundwater and petroleum extraction) (Holzer and Bluntzer, 1984; Morton et al., 2002). According to our field investigations in the Houston area, the damage resulted from fault creeping is mostly limited to a very narrow belt (< 1000 m) along the fault traces (Sanchez, 2013; Serna, 2015). The distribution of current GPS sites in this study may be too sparse to identify fault creeping. In fact, existing CGPS stations are reference stations primarily installed for the purpose of providing stable references for local land surveying community. The locations were selected purposely to avoid known areas affected by faulting.

5 Vertical ground deformation

The overall spatial variation of vertical velocities in the GOM region is much greater compared to that of horizontal velocities. There are certain stations showing extremely large downward vertical velocities in this region. Figure 4b indicates four rapid subsidence zones in the GOM region – the southeastern Louisiana area, the Houston metropolitan area, Aguascalientes, and Mexico City. The drivers of subsidence vary from place to place. Different drivers would result in different subsidence patterns – the

NHESSD
3, 6651–6688, 2015

spatial and temporal variability of subsidence rates. In this section, we discuss subsidence in southeastern Louisiana, Houston, Aguascalientes and Mexico City.

5.1 Subsidence in the southeastern Louisiana

The causes behind present subsidence in southeastern Louisiana have been controversial and heavily studied. Ramsey and Moslow (1987) attributed 80 % of the present subsidence on the coast of Louisiana to "compactional subsidence." Roberts et al. (1994) studied relationships between subsidence rates and faulting, land loss, thickness and characteristics of Holocene sediment in the Louisiana coastal area, and they concluded that sediment compaction was a primary cause of subsidence. A number of studies proposed that the present-day subsidence in the Mississippi Delta is mostly caused by the isostatic response to the delta load (e.g., Ivins et al., 2007; Jurkowski et al., 1984). However, Dokka (2006) argued the conventional opinions; using a case study conducted in the Michoud area of Orleans Parish, Louisiana, Dokka (2006) concluded that 73 % (16.9 mm yr^{-1}) of subsidence during the period 1969–1971 and 50 % (7.1 mm yr^{-1}) of subsidence during the period 1971–1977 was attributed to tectonism (fault movements). Dokka and his colleagues further addressed tectonic-induced subsidence in their other publications (Dixon et al., 2006; Dokka, 2011; Dokka et al., 2006). Wolstencroft et al. (2014) investigated the cause of subsidence in the Mississippi Delta through geophysical modeling and concluded that present-day basement subsidence rate due to sediment loading was less than ~ 0.5 mm yr^{-1} and the glacial isostatic adjustment was likely to be the major driver of deep-seated subsidence.

Figure 9a and c illustrates the velocity vectors and positional time series at long-term GPS stations across the southeastern Louisiana area. Considerable subsidence rates are recorded at two near-coast stations (LMCN, GRIS) (< 10 km to the coastal line). Both sites indicate steady subsidence of approximately 6 mm yr^{-1} over 10 years. Four inland stations FSHS, AWES, HOUM and DSTR show smaller subsidence rates (2–4 mm yr^{-1}). The seaward increase in the rate of subsidence may be a combined result of shallow sediment compaction and deep basement subsidence. The natural

NHESSD
3, 6651–6688, 2015

compaction of young sediments could occur in new infill and recently drained mashes (Törnqvist et al., 2008). GPS stations underlain by shallow (Holocene) sediments in this area will be subject to the ongoing compaction. Wolstencroft et al. (2014) demonstrated that present-day Pleistocene basement subsidence (deep subsidence) in the Mississippi Delta produced by viscoelastic deformation mechanisms also increased seaward.

Compared to near-coast sites LMCN and GRIS, another near-coast GPS site BVHS (2002–2014) recorded a 50 % smaller subsidence rate (3 mm yr^{-1}). This difference may be due to the fact that BVHS is located at a different delta lobe (Balize) with LMCN and GRIS (Ivins et al., 2007). Delta lobes are formed by "delta switching," a systematic change of the sediment deposition caused by river course shifts (Ivins et al., 2007). Modern rates of deposition and sediment loading volume could vary from different delta lobes. The Balize lobe where BVHS is located has a smaller volume of Holocene sediment loading (Ivins et al., 2007). Therefore, there might be less of an isostatic response to the delta load. Despite the different subsidence rates between coastal sites and inland sites, the overall spatial variation of subsidence rates across southeastern Louisiana is relatively small compared to that of the Houston metropolitan area. The slight variation of subsidence rates in space and the steady subsidence in time suggest that the subsidence is not likely dominated by the compaction of shallow aquifers associated with groundwater pumping. Groundwater pumping induced subsidence often shows considerable spatial and/or temporal variations as illustrated by subsidence in the metropolitan area of Houston and Mexico City (discussed in the following sections). In southeast Louisiana, groundwater withdrawal is minimal because groundwater quality is affected by saltwater encroachment (Baumann et al., 2006). The exception is for the greater New Orleans area, where groundwater is pumped from shallow upper Pleistocene aquifers. Spatial correlations between areas of large subsidence and areas with high-yield groundwater wells in the New Orleans area were reported by Dokka (2011).

NHESSD
3, 6651–6688, 2015

5.2 Subsidence in the Houston area

The groundwater induced subsidence in the Houston area has been intensively investigated by researchers from the US Geological Survey (USGS) (Bawden et al., 2012; Galloway et al., 1999; Johnson et al., 2011; Kasmarek et al., 2009, 2010, 2012, 2013), National Geodetic Survey (NGS) (Zilkoski et al., 2003), and local research institutions (e.g., Engelkemeir et al., 2010; Kearns et al., 2015; Khan et al., 2014; Wang and Soler, 2013). A recent study conducted by Yu et al. (2014) indicated that the subsidence in the Houston metropolitan area is attributed by the compaction of aquifers within about 500 m to the ground surface. Since groundwater usage changes accordingly to the local population and land usage, the subsidence resulting from groundwater withdrawal will vary in space. The subsidence rate will also change over time in accordance to the city development and policy changes. Historically, subsidence in the Houston area had been primarily occurring in the eastern and southeastern portions. A comparison of the current subsidence and recent subsidence (1915–2001) mapped by the USGS (Bawden et al., 2012) indicates that the subsidence in the Houston area has been migrating to the western and northern areas since the 1990s. The overall subsidence has also been reduced significantly as a result of rigidly enforced groundwater regulation plans (Harris-Galveston Subsidence District, 2013).

Figure 9b and d illustrates the velocity vectors and positional time series at long-term GPS stations within the Houston area. The spatial variation of subsidence in the Houston area is more significant than that in southeastern Louisiana. The highest subsidence rates in the Houston area are recorded at two inland sites: TXCN and ROD1 (Table 3). These two stations are more than 100 km away from the coastal line. The subsidence rate is as high as 17 mm yr^{-1} at TXCN. Two coastal stations TXGV and TXGA record subsidence rates of only 1.3 and 4.4 mm yr^{-1}, respectively. Considerable temporal variations in subsidence rates are also identified at certain sites. For instance, the subsidence rate at ROD1 was 25 mm yr^{-1} before 2010 and reduced to 13 mm yr^{-1}

NHESSD
3, 6651–6688, 2015

after 2010 due to the enforced groundwater regulation plan at 2010 (Fig. 5) (Harris-Galveston Subsidence District, 2013).

5.3 Salt tectonics

The Gulf Coast area is one of the world's largest salt dome regions. Over 500 salt domes have been discovered onshore and under the sea floor of the GOM (Beckman and Williamson, 1990). Salt movements in the coastal area could exert a large impact on surface morphological features and cause faulting activities in the long-term. The vertical velocity vectors illustrated in this study do not show any considerable vertical movement that can be resulted from salt dome uplift. Jackson and Seni (1983) showed that the maximum net growth rate of diapirs in East Texas is 150 to 230 m per million years, which equals $\sim 0.2\,\mathrm{mm\,yr^{-1}}$. The ground deformation rate at this level is below the limit that can be identified with the current GPS geodesy infrastructure in this region during the observational time period of only a few years.

5.4 Subsidence in central Mexico

The CGPS sites in two central Mexico cities – Aguascalientes and Mexico City show extremely rapid subsidence. The causality between groundwater extraction and land subsidence in Mexico City was first investigated in the 1930s and then the 1940s (Carrillo, 1947; Cuevas, 1936). Groundwater accounts for nearly half of Mexico City's water usage (Sosa-Rodriguez, 2010). As of 2011, shallow aquifers in this region had been seriously overexploited (Engel et al., 2011). The ground water level has been declining at average rates ranging from 0.1 to $1.5\,\mathrm{m\,yr^{-1}}$ in different zones since 1983 (The Joint Academies Committee on the Mexico City Water Supply et al., 1995). Figure 10 illustrates the three-component positional time series at three CGPS sites: INEG, MMX1, and UNIP. INEG is located in the city of Aguascalientes, Mexico. This station shows a steady subsidence rate of $25.7\,\mathrm{mm\,yr^{-1}}$. MMX1 records steady land subsidence at a rate of $266.3\,\mathrm{mm\,yr^{-1}}$, which could be the most rapid subsidence rate ever recorded

NHESSD
3, 6651–6688, 2015

by a CGPS station. The subsidence rate at the center of the subsidence bowl could be even larger. In fact, a subsidence rate as high as 370 mm yr^{-1} (1996–2005) was derived from InSAR studies in Mexico City (Cabral-Cano et al., 2008). UNIP records a small subsidence rate of 2.7 mm yr^{-1}. The distance between MMX1 and UNIP is only about 17.8 km. The subsidence rate at MMX1 is about 100 times higher than that at UNIP. It demonstrates the significant spatial variation of the subsidence rate in Mexico City.

6 Conclusions

This study utilizes the current GPS geodesy infrastructure in the GOM region to investigate the ground deformation associated with subsidence and faulting. A sophisticated regional GPS geodesy infrastructure should include three components: individual GPS stations, a stable local reference frame, and sophisticated positioning software packages. Currently, a unified "local reference frame" does not exist in the GOM region. This study established a stable local reference frame (SGOMRF) to fill the gap. In the first release of the SGOMRF, the 14 Helmert transformation parameters for converting coordinates from the IGS08 to SGOMRF are provided (Table 1). The SGOMRF will be incrementally improved and periodically updated to synchronize with the updates of the IGS reference frame. The potential applications of the local reference frame include providing a consistent framework for precisely monitoring coastal hazards over space and time, conducting risk analysis, studying coastal erosion and wetland loss, studying sea level rise, and comparing research results from different research groups. The stable reference frame will also be useful for long-term health monitoring of dams, sea walls, high-rise buildings, long-span bridges and for planning and designing coastal restoration projects.

GPS observations show significant land subsidence in the coastal area of southeastern Louisiana, the Houston metropolitan area, Aguascalientes, and Mexico City of Mexico. Significant spatial variations of subsidence rates due to differences in ground-

NHESSD
3, 6651–6688, 2015

water usage and clay layer thickness are observed in the Houston area and Mexico City. The decrease of the subsidence rate over time is also observed at CGPS stations located in Houston. The CGPS sites in the southeastern Louisiana area show steady subsidence and a general southward horizontal movement toward the GOM. This may suggest a deep tectonic process associated with faulting. Subsidence resulting from faulting would be difficult to stop through human efforts. As a result, the minor but steady subsidence (4–6 mm yr^{-1}) would cause considerable damage to the coastal protection infrastructure (e.g., sea walls, levees, floodwalls, storm surge barriers) in the long term.

GPS observations presented in this study do not show any considerable vertical ground movements that could be associated with salt tectonics. The magnitude of salt dome uplift may be below the level that can be identified by the current GPS geodesy infrastructure with a time span less than a decade. A denser CGPS network and a longer period of data accumulation are crucial for a more comprehensive study of local ground motions within the GOM region.

Acknowledgements. The authors thank NGS and UNAVCO for providing GPS data to the public. This study was supported by an NSF CAREER award EAR-1229278, an NSF MRI award EAR-1242383, and an NSF TUES award DUE-1243582.

References

Altamimi, Z., Collilieux, X., Legrand, J., Garayt, B., and Boucher, C.: ITRF2005: A new release of the International Terrestrial Reference Frame based on time series of station positions and Earth Orientation Parameters, J. Geophys. Res., 112, B09401, doi:10.1029/2007JB004949, 2007.

Bar-Sever, Y. E., Kroger, P. M., and Borjesson, J. A.: Estimating horizontal gradients of tropospheric path delay with a single GPS receiver, J. Geophys. Res., 103, 5019, doi:10.1029/97JB03534, 1998.

NHESSD

3, 6651–6688, 2015

Baumann, T., Goree, B., Lovelace, W., Montgomery, P., Ross, G., Walters, D., and Ward, A.: Water Resources Data for Louisiana, Water Year 2005, Water-Data Report LA-05-01, US Geological Survey, Baton Rouge, LA, 2006.
Bawden, G., Johnson, M., and Kasmarek, M.: Investigation of land subsidence in the Houston-Galveston region of Texas by using the Global Positioning System and Interferometric Synthetic Aperture Radar, 1993–2000, USGS Scientific Investigation Report 2012-5211, US Geological Survey, Reston, VA, 2012.
Beckman, J. D. and Williamson, A. K.: Salt-dome locations in the Gulf Coastal Plain, South-Central United States, Water-Resources Investig. Rep., US Geological Survey, Austin, TX, 1990.
Bertiger, W., Desai, S. D., Haines, B., Harvey, N., Moore, A. W., Owen, S., and Weiss, J. P.: Single receiver phase ambiguity resolution with GPS data, J. Geod., 84, 327–337, doi:10.1007/s00190-010-0371-9, 2010.
Blewitt, G. and Lavallée, D.: Effect of annual signals on geodetic velocity, J. Geophys. Res. Solid Earth, 107, ETG 9-1–ETG 9-11, doi:10.1029/2001JB000570, 2002.
Boehm, J., Niell, A., Tregoning, P., and Schuh, H.: Global Mapping Function (GMF): a new empirical mapping function based on numerical weather model data, Geophys. Res. Lett., 33, L07304, doi:10.1029/2005GL025546, 2006.
Cabral-Cano, E., Dixon, T. H., Miralles-Wilhelm, F., Diaz-Molina, O., Sanchez-Zamora, O., and Carande, R. E.: Space geodetic imaging of rapid ground subsidence in Mexico City, Geol. Soc. Am. Bull., 120, 1556–1566, doi:10.1130/B26001.1, 2008.
Canny, J.: A computational approach to edge detection, IEEE Trans. Pattern Anal. Mach. Intell., 8, 679–698, doi:10.1109/TPAMI.1986.4767851, 1986.
Carrillo, N.: Influence of Artesian Wells in the Sinking of Mexico City, in: Comision Impulsora y Coordinadora de la Investigacion Cientifica, vol. 47, Secretaria de Hacienda y Credito Publico, Mexico, D.F., 7–14, 1947.
Chaussard, E., Wdowinski, S., Cabral-Cano, E., and Amelung, F.: Land subsidence in central Mexico detected by ALOS InSAR time-series, Remote Sens. Environ., 140, 94–106, doi:10.1016/j.rse.2013.08.038, 2014.
Collilieux, X., Métivier, L., Altamimi, Z., Dam, T., and Ray, J.: Quality assessment of GPS reprocessed terrestrial reference frame, GPS Solut., 15, 219–231, doi:10.1007/s10291-010-0184-6, 2010.

NHESSD
3, 6651–6688, 2015

Cuevas, J.: Foundation Conditions in Mexico City, in: Proceedings of International Conference on Soil Mechanics, International Society for Soil Mechanics and Geotechnical Engineering, Cambridge, Mass., 233–237, 1936.
Day, J. W., Pont, D., Hensel, P. F., Ibañez, C., and Ibanez, C.: Impacts of sea-level rise on deltas in the Gulf of Mexico and the Mediterranean: the importance of pulsing events to sustainability, Estuaries, 18, 636–647, doi:10.2307/1352382, 1995.
DeMets, C., Gordon, R. G., Argus, D. F., and Stein, S.: Current plate motions, Geophys. J. Int., 101, 425–478, doi:10.1111/j.1365-246X.1990.tb06579.x, 1990.
Dixon, T. H., Amelung, F., Ferretti, A., Novali, F., Rocca, F., Dokka, R., Sella, G., Kim, S.-W., Wdowinski, S., and Whitman, D.: Space geodesy: subsidence and flooding in New Orleans, Nature, 441, 587–588, doi:10.1038/441587a, 2006.
Dokka, R. K.: Modern-day tectonic subsidence in coastal Louisiana, Geology, 34, 281–284, doi:10.1130/G22264.1, 2006.
Dokka, R. K.: The role of deep processes in late 20th century subsidence of New Orleans and coastal areas of southern Louisiana and Mississippi, J. Geophys. Res., 116, B06403, doi:10.1029/2010JB008008, 2011.
Dokka, R. K., Sella, G. F., and Dixon, T. H.: Tectonic control of subsidence and southward displacement of southeast Louisiana with respect to stable North America, Geophys. Res. Lett., 33, L23308, doi:10.1029/2006GL027250, 2006.
Engel, K., Jokiel, D., Kraljevic, A., and Geiger, M.: Big Cities. Big Water. Big Challenges. Water in an urbanizing world, WWF Germany, Berlin, 2011.
Engelkemeir, R., Khan, S. D., and Burke, K.: Surface deformation in Houston, Texas using GPS, Tectonophysics, 490, 47–54, 2010.
Firuzabadì, D. and King, R. W.: GPS precision as a function of session duration and reference frame using multi-point software, GPS Solut., 16, 191–196, doi:10.1007/s10291-011-0218-8, 2011.
Galloway, D., Jones, D., and Ingebritsen, S.: Land subsidence in the United States, USGS Circular 1182, US Geological Survey, Reston, VA, 1999.
Garrity, C. and Soller, D.: Database of the Geologic Map of North America; adapted from the map by: Reed Jr., J. C. and others (2005), US Geol. Surv. Data Ser. 424, US Geological Survey, Reston, VA, 2009.

NHESSD
3, 6651–6688, 2015

Harris–Galveston Subsidence District: Harris–Galveston Subsidence District Regulatory Plan 2013, Adopted 9 January 2013, Amended 8 May 2013, Harris–Galveston Subsidence District, Friendswood, TX, 2013.

Holzer, T. L. and Bluntzer, R. L.: Land subsidence near oil and gas fields, Houston, Texasa, Ground Water, 22, 450–459, doi:10.1111/j.1745-6584.1984.tb01416.x, 1984.

Ivins, E. R., Dokka, R. K., and Blom, R. G.: Post-glacial sediment load and subsidence in coastal Louisiana, Geophys. Res. Lett., 34, L16303, doi:10.1029/2007GL030003, 2007.

Jackson, M. P. A. and Seni, S. J.: Geometry and evolution of salt structures in a marginal rift basin of the Gulf of Mexico, east Texas, Geology, 11, 131–135, doi:10.1130/0091-7613(1983)11<131:GAEOSS>2.0.CO;2, 1983.

Johnson, M. R., Ramage, J. K., and Kasmarek, M. C.: Water-level altitudes 2011 and water-level changes in the Chicot, Evangeline, and Jasper aquifers and compaction 1973–2010 in the Chicot and Evangeline aquifers, Houston–Galveston region, Texas, USGS Sci. Invest. Map 3174, US Geological Survey, Reston, VA, 2011.

Jurkowski, G., Ni, J., and Brown, L.: Modern uparching of the Gulf Coastal Plain, J. Geophys. Res., 89, 6247, doi:10.1029/JB089iB07p06247, 1984.

Kasmarek, M. C., Gabrysch, R. K., and Johnson, M. R.: Estimated land-surface subsidence in Harris County, Texas, 1915–17 to 2001, USGS Sci. Invest. Map 3097, US Geological Survey, Reston, VA, 2009.

Kasmarek, M. C., Johnson, M. R., and Ramage, J. K.: Water-level altitudes 2010 and water-level changes in the Chicot, Evangeline, and Jasper aquifers and compaction 1973–2009 in the Chicot and Evangeline aquifers, Houston–Galveston region, Texas., USGS Sci. Invest. Map 3138, US Geological Survey, Reston, VA, 2010.

Kasmarek, M. C., Johnson, M. R., and Ramage, J. K.: Water-level altitudes 2012 and water-level changes in the Chicot, Evangeline, and Jasper aquifers and compaction 1973–2011 in the Chicot and Evangeline aquifers, Houston–Galveston region, Texas, USGS Sci. Invest. Map 3230, US Geological Survey, Reston, VA, 2012.

Kasmarek, M. C., Johnson, M. R., and Ramage, J. K.: Water-level altitudes 2013 and water-level changes in the Chicot, Evangeline, and Jasper aquifers and compaction 1973–2012 in the Chicot and Evangeline aquifers, Houston-Galveston region, Texas, USGS Sci. Invest. Map 3263, US Geological Survey, Reston, VA, 2013.

NHESSD
3, 6651–6688, 2015

Kearns, T. J., Wang, G., Bao, Y., Jiang, J., and Lee, D.: Current Land Subsidence and Groundwater Level Changes in the Houston Metropolitan Area (2005–2012), J. Surv. Eng., 141, 05015002, doi:10.1061/(ASCE)SU.1943-5428.0000147, 2015.
Kedar, S.: The effect of the second order GPS ionospheric correction on receiver positions, Geophys. Res. Lett., 30, 1829, doi:10.1029/2003GL017639, 2003.
Khan, S. D., Huang, Z., and Karacay, A.: Study of ground subsidence in northwest Harris county using GPS, LiDAR, and InSAR techniques, Nat. Hazards, 73, 1143–1173, doi:10.1007/s11069-014-1067-x, 2014.
Kolker, A. S., Allison, M. A., and Hameed, S.: An evaluation of subsidence rates and sea-level variability in the northern Gulf of Mexico, Geophys. Res. Lett., 38, L21404, doi:10.1029/2011GL049458, 2011.
Lyard, F., Lefevre, F., Letellier, T., and Francis, O.: Modelling the global ocean tides: modern insights from FES2004, Ocean Dyn., 56, 394–415, doi:10.1007/s10236-006-0086-x, 2006.
Morton, R. A., Buster, N. A., Krohn, M. D., and Ruppel, S.: Subsurface controls on historical subsidence rates and associated wetland loss in Southcentral Louisiana, Trans. Gulf Coast Assoc. Geol. Soc., 52, 767–778, 2002.
Osmanoglu, B., Dixon, T. H., Wdowinski, S., Cabral-Cano, E., and Jiang, Y.: Mexico City subsidence observed with persistent scatterer InSAR, Int. J. Appl. Earth Obs. Geoinf., 13, 1–12, doi:10.1016/j.jag.2010.05.009, 2011.
Pearson, C. and Snay, R.: Introducing HTDP 3.1 to transform coordinates across time and spatial reference frames, GPS Solut., 17, 1–15, doi:10.1007/s10291-012-0255-y, 2012.
Ramsey, K. E. and Moslow, T. F.: A Numerical Analysis of Subsidence and Sea Level Rise in Louisiana, in: Proceedings of Coastal Sediments '87, American Society of Civil Engineers, New Orlean, LA, 1673–1688, 1987.
Rebischung, P., Griffiths, J., Ray, J., Schmid, R., Collilieux, X., and Garayt, B.: IGS08: the IGS realization of ITRF2008, GPS Solut., 16, 483–494, doi:10.1007/s10291-011-0248-2, 2012.
Roberts, H. H., Bailey, A., and Kuecher, G. J.: Subsidence in the Mississippi River Delta; important influences of valley filling by cyclic deposition, primary consolidation phenomena, and early diagenesis, Trans. Gulf Coast Assoc. Geol. Soc., 44, 619–629, 1994.
Sanchez, G.: Determing the Trace and Kinematics of the Long Point Fault in Houston, Texas using LiDAR data and Continuous GPS Monitoring, MS thesis, University of Houston, Houston, TX, 2013.

NHESSD
3, 6651–6688, 2015

Schwarz, C.: The North American Datum of 1983, NOAA Professional Paper NOS 2, National Geodetic Information Branch, NOAA, Rockville, MD, 1989.
Serna, J.: Current Ground Motions Along the Long-Point Fault Derived from Continous GPS Observations 2012–2104, MS thesis, University of Houston, Houston, TX, 2015.
Simms, A. R., Anderson, J. B., DeWitt, R., Lambeck, K., and Purcell, A.: Quantifying rates of coastal subsidence since the last interglacial and the role of sediment loading, Global Planet. Change, 111, 296–308, 2013.
Snay, R. and Soler, T.: Modern terrestrial reference systems. Part 2: The evolution of the NAD83, Prof. Surv., 20, 16–18, 2000.
Sosa-Rodriguez, F.: Exploring the risks of ineffective water supply and sewage disposal: a case study of Mexico City, Environ. Hazards, 9, 135–146, doi:10.3763/ehaz.2010.0016, 2010.
Thatcher, C. A., Brock, J. C., and Pendleton, E. A.: Economic vulnerability to sea-level rise along the Northern US Gulf Coast, J. Coast. Res. Spec. Issue 63 – Underst. Predict. Chang. Coast. Ecosyst. North. Gulf Mex., 234–243, doi:10.2112/SI63-017.1, 2013.
The free ocean tide loading provider: http://holt.oso.chalmers.se/loading/index.html, last access: 15 January 2015.
The Joint Academies Committee on the Mexico City Water Supply, Environment and Resources Commission on Geosciences, National Research Council, A. C. Academia Nacional de la Investigacion Cientifica and A. C. Academia Nacional de Ingenieria: Mexico City's Water Supply: Improving the Outlook for Sustainability, The National Academies Press, Washington, D.C., 1995.
Törnqvist, T. E., Wallace, D. J., Storms, J. E. A., Wallinga, J., van Dam, R. L., Blaauw, M., Derksen, M. S., Klerks, C. J. W., Meijneken, C., and Snijders, E. M. A.: Mississippi Delta subsidence primarily caused by compaction of Holocene strata, Nat. Geosci., 1, 173–176, doi:10.1038/ngeo129, 2008.
Verbeek, E. R., Ratzlaff, K. W., and Clanton, U. S.: Faults in parts of north-central and western Houston metropolitan area, Texas, Miscellaneous Field Studies Map 1136, US Geological Survey, Reston, VA, 1979.
Wang, G.: GPS landslide monitoring: single base vs. network solutions – a case study based on the Puerto Rico and Virgin Islands Permanent GPS Network, J. Geod. Sci., 1, 191–203, doi:10.2478/v10156-010-0022-3, 2011.
Wang, G. and Soler, T.: Using OPUS for measuring vertical displacements in Houston, TX, J. Surv. Eng., 139, 126–134, doi:10.1061/(ASCE)SU.1943-5428.0000103, 2013.

NHESSD
3, 6651–6688, 2015

Wang, G. and Soler, T.: Measuring land subsidence using GPS: ellipsoid height versus orthometric height, J. Surv. Eng., 14, 05014004-1–05014004-12, doi:10.1061/(ASCE)SU.1943-5428.0000137, 2014.
Wang, G., Yu, J., Ortega, J., Saenz, G., Burrough, T., and Neill, R.: A stable reference frame for the study of ground deformation in the Houston Metropolitan Area, Texas, J. Geod. Sci., 3, 188–202, doi:10.2478/jogs-2013-0021, 2013.
Wang, G., Kearns, T. J., Yu, J., and Saenz, G.: A stable reference frame for landslide monitoring using GPS in the Puerto Rico and Virgin Islands region, Landslides, 11, 119–129, doi:10.1007/s10346-013-0428-y, 2014.
Wang, G., Bao, Y., Cuddus, Y., Jia, X., Serna, J., and Jing, Q.: A methodology to derive precise landslide displacement time series from continuous GPS observations in tectonically active and cold regions: a case study in Alaska, Nat. Hazards, 77, 1939–1961, doi:10.1007/s11069-015-1684-z, 2015.
Williams, S., Stone, G., and Burruss, A.: A perspective on the Louisiana wetland loss and coastal erosion problem, J. Coast. Res., 13, 593–594, 1997.
Wolstencroft, M., Shen, Z., Törnqvist, T. E., Milne, G. A., and Kulp, M.: Understanding subsidence in the Mississippi Delta region due to sediment, ice, and ocean loading: insights from geophysical modeling, J. Geophys. Res.-Solid, 119, 3838–3856, doi:10.1002/2013JB010928, 2014.
Worral, D. and Sigmund, S.: Evolution of the northern Gulf of Mexico, with emphasis on Cenozoic growth faulting and the role of salt, in: The Geology of North America – An Overview, Geological Society of America, edited by: Bally, A. and Palmer, A., Geological Society of America, Boulder, CO, 97–138, 1989.
Yu, J., Wang, G., Kearns, T. J., and Yang, L.: Is there deep-seated subsidence in the Houston-Galveston Area?, Int. J. Geophys., 2014, 942834, doi:10.1155/2014/942834, 2014.
Zilkoski, D., Hall, L., Mitchell, G., Kammula, V., Singh, A., Chrismer, W., and Neighbors, R.: The Harris-Galveston Coastal Subsidence District/National Geodetic Survey automated Global Positioning System subsidence monitoring Project, in: Proceedings of the US Geological Survey Subsidence Interest Group Conference, US Geological Survey, Galveston, TX, 13–28, 2003.
Zumberge, J. F., Heflin, M. B., Jefferson, D. C., Watkins, M. M., and Webb, F. H.: Precise point positioning for the efficient and robust analysis of GPS data from large networks, J. Geophys. Res., 102, 5005–5017, doi:10.1029/96JB03860, 1997.

NHESSD
3, 6651–6688, 2015

Table 1. Fourteen parameters for reference frame transformations from IGS08 to SGOMRF and from IGS08 to NAD83 (2011).

Parameter	Unit	IGS08 to SGOMRF t_0 = 2013.0	IGS08 to NAD83(2011)[a] t_0 = 1997.0
$T_x(t_0)$	cm	0.00000	99.34300
$T_y(t_0)$	cm	0.00000	−190.33100
$T_z(t_0)$	cm	0.00000	−52.65500
$R_x(t_0)$[b]	mas[c]	0.00000	25.91467
$R_y(t_0)$	mas	0.00000	9.42645
$R_z(t_0)$	mas	0.00000	11.59935
$s(t_0)$	ppb[d]	0.00000	1.71504
dT_x	cm yr^{-1}	0.24978	0.07900
dT_y	cm yr^{-1}	−0.12958	−0.06000
dT_z	cm yr^{-1}	−0.24124	−0.13400
dR_x	mas yr^{-1}	0.10195	0.06667
dR_y	mas yr^{-1}	−0.61808	−0.75744
dR_z	mas yr^{-1}	−0.00673	−0.05133
ds	ppb yr^{-1}	0.04980	−0.10201

[a] Source: Pearson and Snay (2012), Table 7.
[b] Counterclockwise rotations of axes are positive.
[c] mas = milliarc second. Radians to mas coefficient: 206264806.24709636; mas to radians coefficient: 4.848137E-09.
[d] ppb = parts per billion.

NHESSD
3, 6651–6688, 2015

Table 2. Geodetic coordinates (longitude, latitude, ellipsoidal height) of the 13 reference sites with respect to SGOMRF and their RMS accuracy (repeatability).

Geodetic coordinates (SGOMRF)				RMS accuracy		
Station	Longitude (degree)	Latitude (degree)	Ellipsoid height (m)	NS (mm)	EW (mm)	UD (mm)
AL20	−87.663	34.710	131.934	1.93	1.75	7.76
ARLR	−92.383	34.673	73.224	1.98	1.36	6.94
GNVL	−82.277	29.687	22.434	1.74	1.70	5.90
GAMC	−83.649	32.702	91.395	1.94	1.72	7.29
MTY2	−100.313	25.716	521.864	1.97	2.09	6.31
OKAN	−95.621	34.195	140.296	1.76	1.81	6.49
OKAR	−97.169	34.168	235.819	1.83	2.67	6.55
RMND	−80.384	25.614	−15.684	1.88	1.94	6.96
TAM1	−97.864	22.278	21.043	1.98	2.06	6.13
TXDC	−97.609	33.236	255.341	1.90	1.84	6.15
TXSA	−100.473	31.414	566.086	2.08	1.86	6.25
TXSN	−102.409	30.153	850.957	1.76	1.90	6.04
TXST	−98.182	32.233	376.569	1.74	1.85	5.92
Average				1.88	1.89	6.51

NHESSD
3, 6651–6688, 2015

Table 3. Horizontal (V_h) and vertical velocities (V_v) of GPS stations plotted in Fig. 9.

Houston			Southeastern Louisiana		
Reference frame: SGOMRF			Reference frame: SGOMRF		
Station	V_h (mm yr^{-1})	V_v (mm yr^{-1})	Station	V_h (mm yr^{-1})	V_v (mm yr^{-1})
ROD1	2.33	−17.32	LMCN	0.94	−6.30
TXCN	0.56	−16.38	GRIS	0.46	−5.93
ZHU1	0.80	−10.80	AWES	0.74	−3.76
COH6	1.72	−8.10	HOUM	0.96	−3.62
TXHE	0.94	−7.51	FSHS	3.49	−3.33
TXLM	1.90	−5.03	BVHS	0.82	−3.02
DWI1	0.98	−4.63	DSTR	0.42	−1.74
TXGA	0.12	−4.36			
ANG6	1.35	−2.57			
TXGV	0.66	−1.34			
TXLI	0.44	−0.44			

NHESSD
3, 6651–6688, 2015

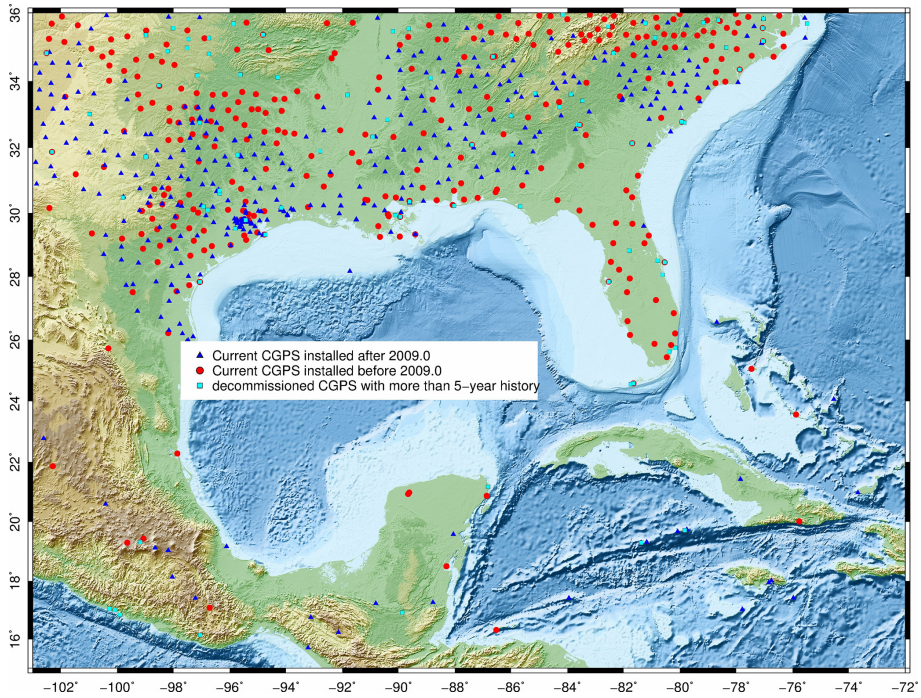

Figure 1. Map showing current CGPS stations in the GOM region. Blue triangles represent current CGPS installed in and after 2009. Red circles represent current CGPS installed before 2009. Grey squares represent decommissioned CGPS that have data spanned for more than 5 years. Data are available through NGS and UNAVCO.

NHESSD
3, 6651–6688, 2015

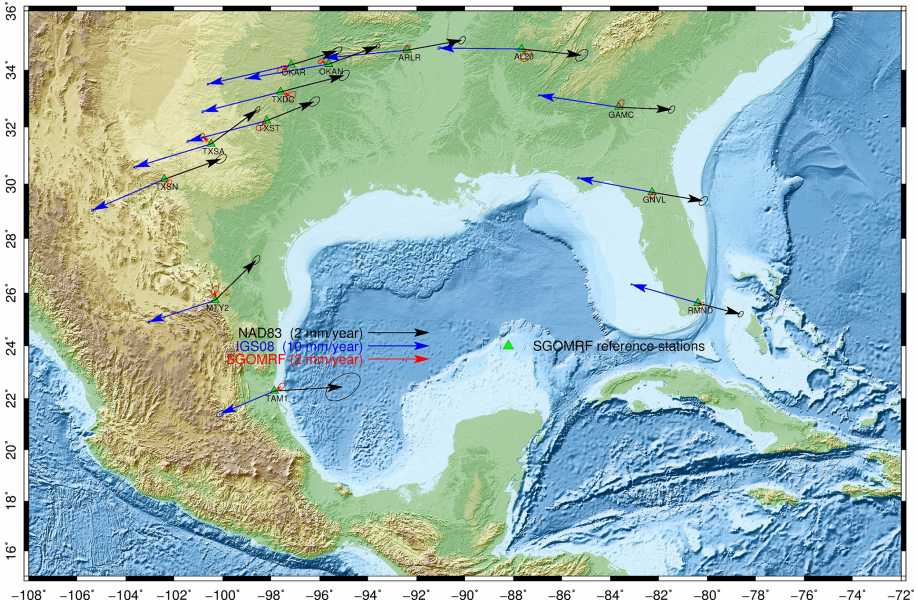

Figure 2. Map showing the locations and velocity vectors with 95 % confidence ellipses of the 13 reference stations used to define SGOMRF. Black vectors are referred to NAD83; blue vectors are referred to IGS08; red vectors are referred to SGOMRF.

NHESSD
3, 6651–6688, 2015

GPS derived ground motions (2005–2014) within the Gulf of Mexico region

J. Yu and G. Wang

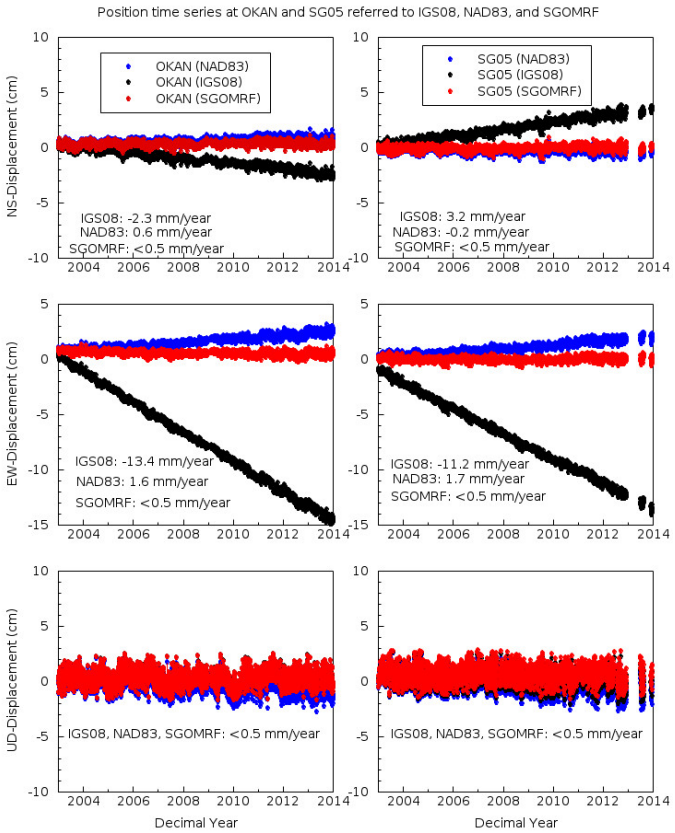

Figure 3. Comparisons of time series at two CGPS sites, OKAN and SG05, referred to three reference frames: IGS08 (black), NAD83 (blue), and SGOMRF (red). OKAN is located at Antlers, Oklahoma. SG05 is located at Melbourne, Florida.

NHESSD
3, 6651–6688, 2015

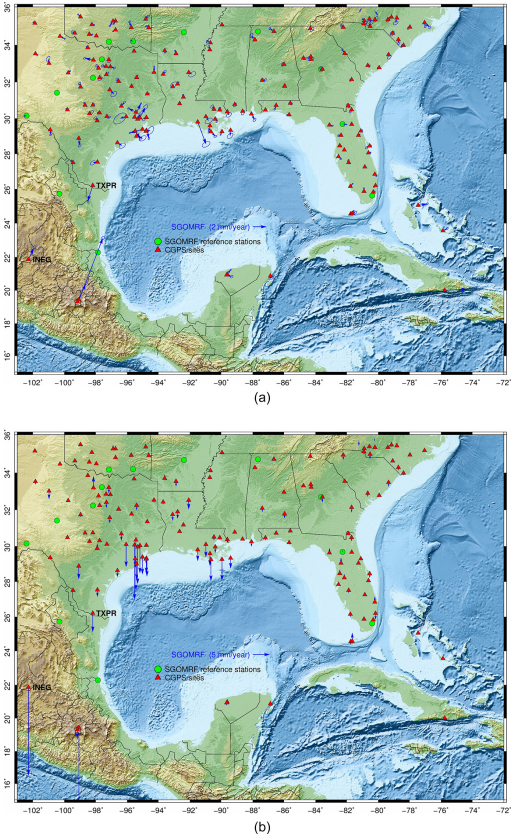

Figure 4. (a) Horizontal velocity with 95 % confident ellipses and **(b)** vertical velocity vectors of 148 CGPS stations (> 4 years) in the Gulf of Mexico region. Green dots represent the 13 reference stations. The blue vectors represent the average velocities referred to SGOMRF.

NHESSD
3, 6651–6688, 2015

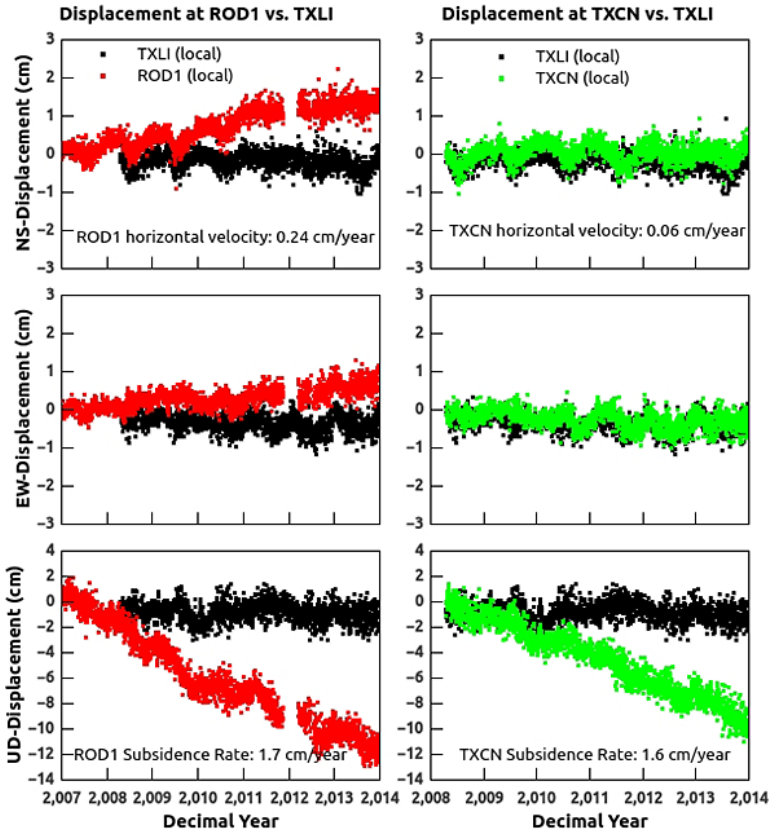

Figure 5. Displacement time series of two rapidly subsiding CGPS sites (ROD1 and TXCN) in northern Houston. The displacement time series of a stable site (TXLI) are plotted for comparative purposes. Locations of these three stations are plotted in Fig. 6. The reference frame is SGOMRF.

NHESSD
3, 6651–6688, 2015

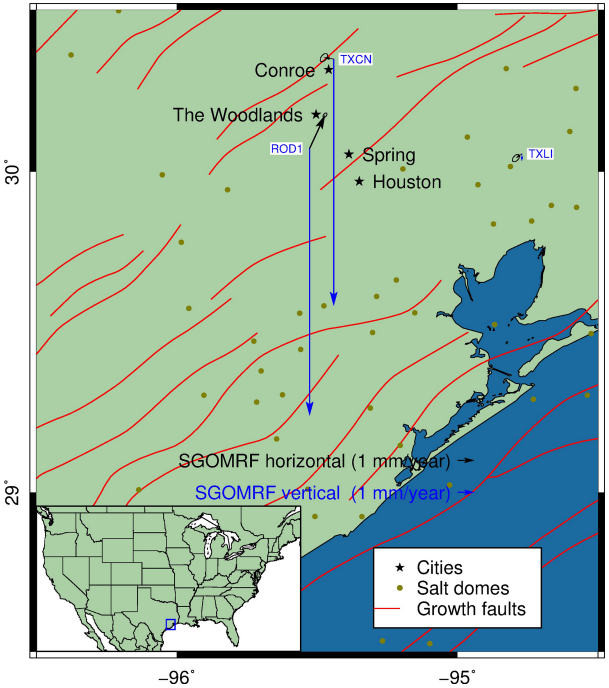

Figure 6. Locations of three CGPS stations and cities within the greater Houston area. Black and blue velocity vectors represent horizontal and vertical velocities with respect to SGOMRF, respectively. Red lines are growth faults and yellow dots are salt domes (Garrity and Soller, 2009).

NHESSD
3, 6651–6688, 2015

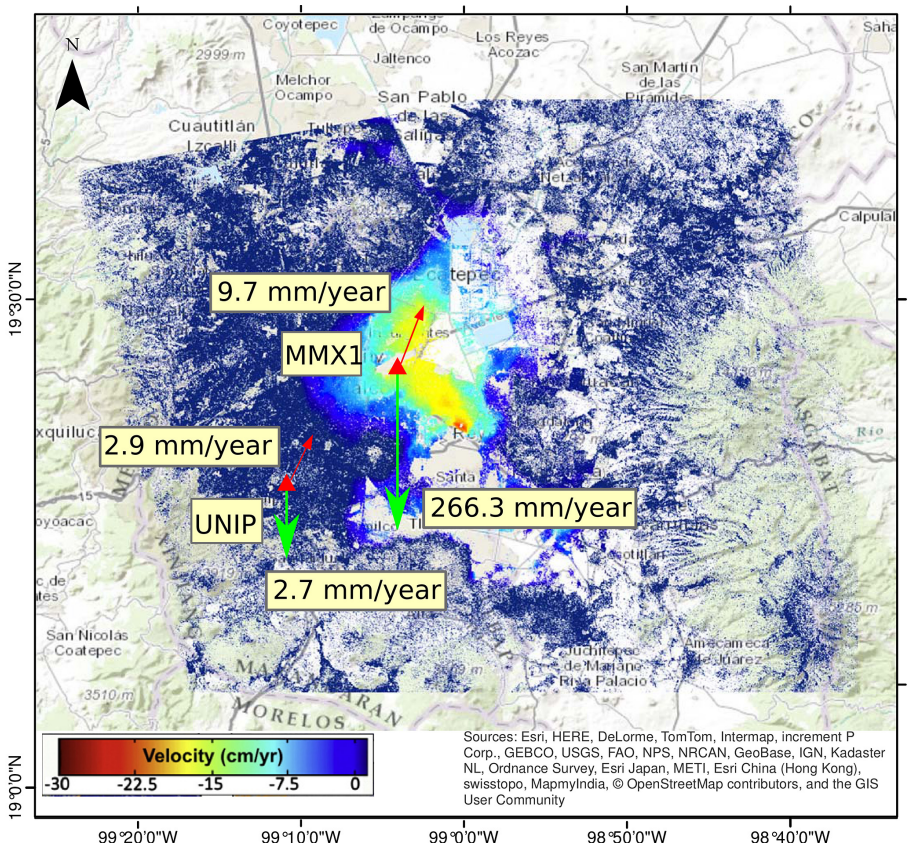

Figure 7. Horizontal (red) and vertical (green) velocity vectors at MMX1 and UNIP with respect to the local reference fame (SGOMRF). The color patterns represent the average subsidence rate derived from InSAR analysis (Chaussard et al., 2014). The three-component positional time series of UNIP and MMXI are plotted in Fig. 10.

NHESSD
3, 6651–6688, 2015

GPS derived ground motions (2005–2014) within the Gulf of Mexico region

J. Yu and G. Wang

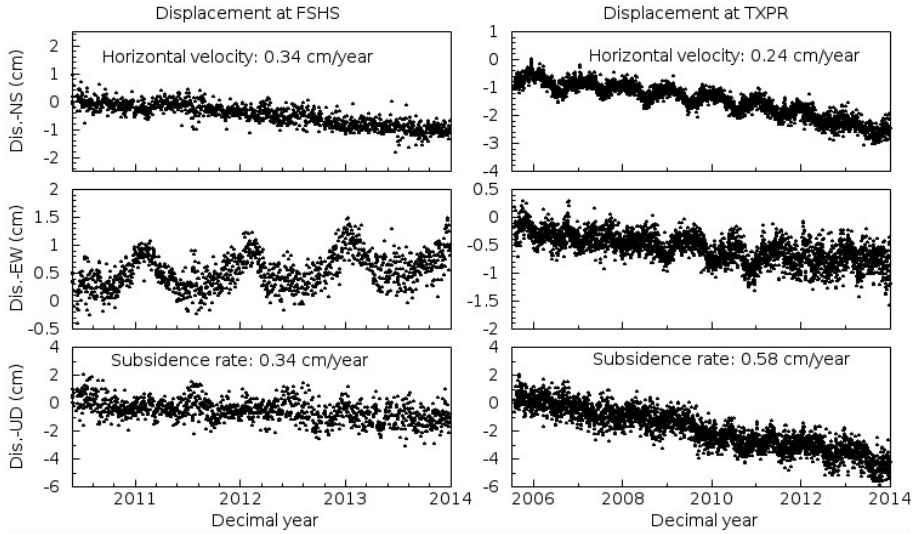

Figure 8. Three-component displacement time series from two CGPS sites with considerable horizontal movements. FSHS is located at Franklin, Louisiana (Fig. 9a). TXPR is located at Pharr, Texas (Fig. 4). The reference frame is SGOMRF.

NHESSD
3, 6651–6688, 2015

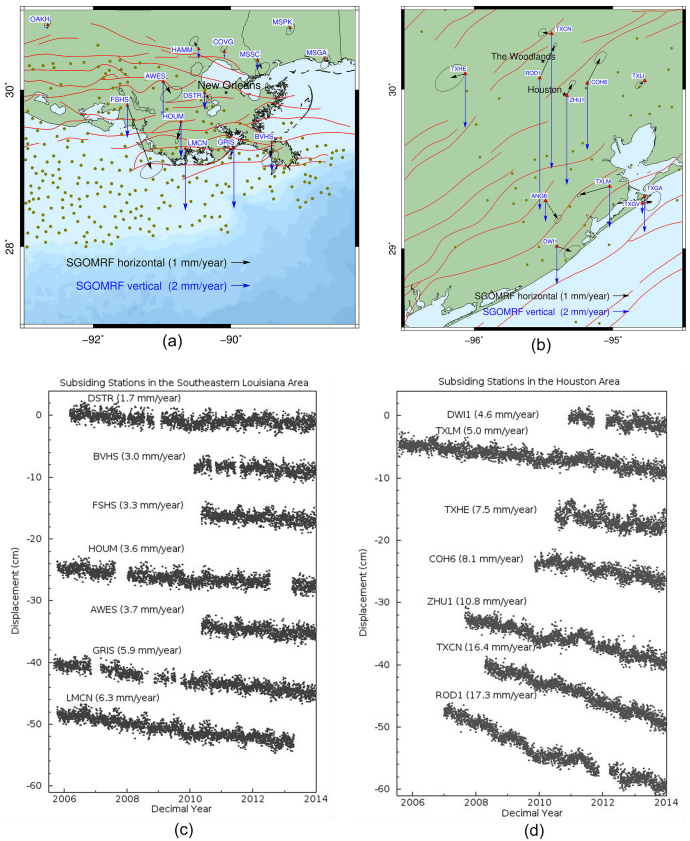

Figure 9. Top maps show vertical and horizontal velocity vectors in **(a)** southeastern Louisiana and **(b)** Houston. Bottom plots show vertical positional time series of subsiding stations in **(c)** southeastern Louisiana ($> 1.5\,\mathrm{mm\,yr^{-1}}$) and **(d)** Houston-Galveston ($> 4.5\,\mathrm{mm\,yr^{-1}}$). The reference frame is SGOMRF.

NHESSD
3, 6651–6688, 2015

GPS derived ground motions (2005–2014) within the Gulf of Mexico region

J. Yu and G. Wang

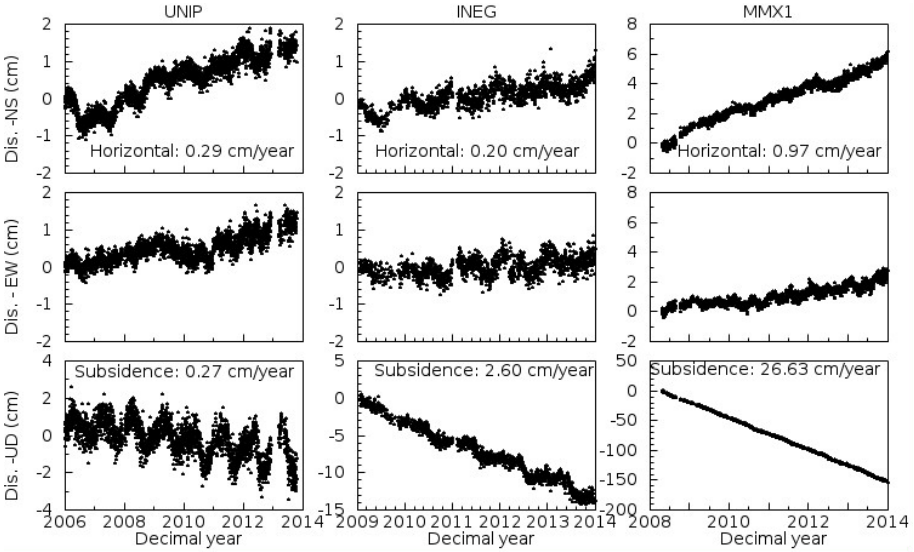

Figure 10. Three-component displacement time series of three CGPS stations in central Mexico. The reference frame is SGOMRF. The locations of UNIP and MMX1 are marked in Fig. 7 and the location of INEG is marked in Fig. 4.

NHESSD
3, 6651–6688, 2015